ECLOUD in PS2, PS+, SPS+*

M. A. Furman,† Center for Beam Physics, LBNL, CA 94720-8211, USA

Abstract

We present a preliminary but broad assessment of the ecloud build-up for the various proposed upgrades of the LHC and its injectors. The study pertains only to the ecloud in bending dipole magnets, and does not shed any light on the effects of the electrons on the beam. We focus on the ecloud heat load, although we have computed many other quantities of interest. The basic variable used to classify our results is the bunch spacing t_b, whose values are 12.5, 25, 50 and 75 ns. The ecloud heat load follows an inverse relation to t_b both for the LHC and for the injectors, with $t_b = 12.5$ ns being by far the least favorable case. Although $t_b = 75$ ns is the most favorable case, the 50-ns option comes closely behind. A simulated comparison of copper vs. stainless steel shows a clear advantage of the former over the latter. Somewhat surprisingly, a comparison of gaussian vs. flat longitudinal bunch profile does not show a clear winner, at least for the LHC at $t_b = 50$ ns. We describe the strengths and limitations of our calculations.

ASSUMPTIONS

We have carried out a preliminary set of simulations of the build-up of the electron cloud for various options considered for the LHC upgrade and its injectors. We have assumed beam and machine parameters as specified in the files "psplusetcparameters" and "lhcupgradeparams" posted on the LUMI2006 website [1]. Our simulations, obtained with the code POSINST [2–5], pertain only to the build-up of the ecloud in a dipole bending magnet for each machine, at a magnetic field B corresponding to the specified beam energy E_b. We have not examined any other regions of the machine, nor any effects from the ecloud on the beam.

Beam We have considered 4 values for the bunch spacing t_b, namely $t_b = 12.5$, 25, 50 and 75 ns. The bunch intensity N_b, RMS bunch length σ_z and longitudinal beam profile are correlated with t_b according to the above-mentioned files except that, for the LHC proper, we have examined the dependence on N_b around its design value while keeping all other variables fixed. For the cases with $t_b = 12.5$ and 25 ns, the assumed longitudinal bunch profile is gaussian, while for $t_b = 50$ and 75 ns it is flat. Our definition of a "flat" longitudinal profile is specified by the line density

$$\lambda(z) = K\left(1 - |z/a|^{1/p}\right)^q\ ,\ |z| < a\ ,\ p, q \geq 0 \qquad (1)$$

where K is a normalization constant. This distribution has a full width $\mathrm{FW} = 2a$, a full width at half maximum FWHM given by

$$\frac{\mathrm{FWHM}}{\mathrm{FW}} = \left(1 - 2^{-1/q}\right)^p \qquad (2)$$

and a RMS length σ_z given by

$$\frac{\sigma_z}{\mathrm{FW}} = \frac{1}{2}\sqrt{\frac{\Gamma(3p)\Gamma(p+q+1)}{\Gamma(p)\Gamma(3p+q+1)}} \qquad (3)$$

The limit of a perfectly flat, or "box," distribution (FWHM=FW) in $-a < z < a$ is obtained by either taking the limit $p \to 0$ with $q \neq 0$, or $q \to 0$ with $p \neq 0$, which yields the well-known result $\sigma_z/\mathrm{FW} = (12)^{-1/2} = 0.29$. For our present purposes we assume that a reasonable description of a flat bunch is given by $\mathrm{FWHM}/\mathrm{FW} = 0.9$ and $q = 10$. These choices lead to $p = 0.039$ and $\sigma_z/\mathrm{FW} = 0.26$. Such a profile is shown in Fig. 1.

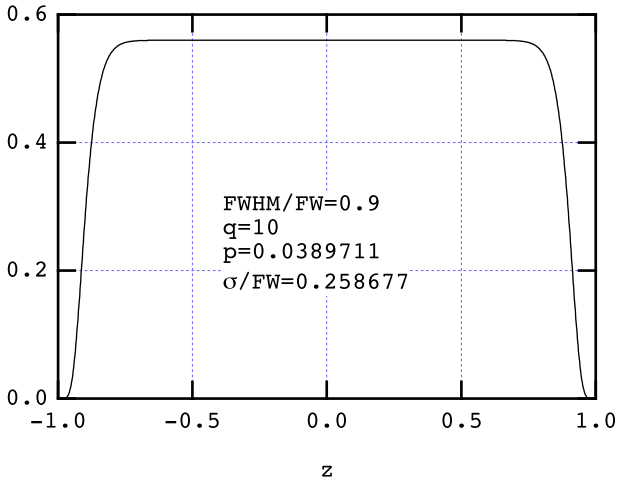

Figure 1: The function $K(1 - |z/a|^{1/p})^q$, normalized to unit area, for $a = 1$, $q = 10$ and FWHM/FW=0.9.

All our results have been obtained by averaging the appropriate ecloud quantities over the first "batch" of the beam injected into an empty machine. The definition of a "batch" depends on t_b, and is as follows:

- $t_b = 12.5$ ns: 144 bunches followed by a gap, for a total of 2 μs.
- $t_b = 25$ ns: 72 bunches followed by a gap, for a total of 2 μs.
- $t_b = 50$ ns: 36 bunches followed by a gap, for a total of 2 μs.
- $t_b = 75$ ns: 24 bunches followed by a gap, for a total of 2 μs.

* Work supported by the U.S. DOE under Contract No. DE-AC02-05CH11231 and by the US-LHC Accelerator Research Project (LARP). Invited paper, Proc. LHC LUMI 2006 (Valencia, Spain, 16–20 October 2006).

† mafurman@lbl.gov

Chamber For the LHC and its upgrades we have assumed the same chamber shape as we have in the past, namely an ellipse with semi-axes $(a, b) = (2.2, 1.8)$ cm [6]. This shape is a reasonable approximation to the real shape, namely round with flattened top and bottom [7]. For the PS and SPS we have assumed a rectangular chamber cross section with half-width and half-height (a, b) as listed in "psplusetcparameters." We have assumed that the surface material is copper for the LHC and stainless steel for the injectors, with SEY model parameters as described in [4, 5]. However, when we explore here the sensitivity of our results to the peak SEY value $\delta_{\max}$, we scale all components of the secondary emission spectrum by a common factor in order to achieve the specified value of $\delta_{\max}$.

For the LHC and its upgrades, the ecloud build-up is seeded predominantly by photoelectrons emitted off the chamber walls by the synchrotron radiation emitted by the beam. The photoemission yield, as well as the value $E_{\max}$ of the incident electron energy at which the SEY has a peak, have an assumed mild dependence on $\delta_{\max}$ as explained in Ref. 7, especially Table II. For the case of stainless steel, we have kept $E_{\max}$ fixed at 310 eV, independent of $\delta_{\max}$.

For the injectors, we have assumed that the dominant mechanism for primary electron generation is ionization of the residual gas. In order to accelerate the simulation of the ecloud build-up, we have assumed for all injector simulations a temperature $T = 300$ K and a residual gas pressure $P = 10^{-5}$ Torr. Such an artificially high value for P is discussed below.

Simulation The results presented in our talk at the LUMI2006 workshop [1] were carried out with rather coarse time steps. Specifically, for those initial simulations, we chose to divide the bunch length into 20 steps for all cases with gaussian profile, and 50 steps for all flat bunch cases (for a gaussian bunch, we always define the full bunch length to be $5\sigma_z$). Those choices translated into values for Δt in the range of $\sim 0.1 - 0.3$ ns. Since the workshop, we have repeated and extended the simulations, whose results are presented below, by dividing the bunch length into a variable number of steps in the range of 50–200, resulting in a time step Δt in the range of $\sim 0.02 - 0.07$ ns. Although the new simulations with smaller Δt are far less noisy than the old ones, and yield more favorable results vis-à-vis the ecloud heat load, we have not methodically studied their numerical convergence as a function of Δt.

In all cases we represent primary electrons by 1,000 macroparticles per bunch passage, and we set an upper limit of 20,000 for the number of macroparticles M_e allowed in the simulation at any given time. In earlier simulations [7] these values were shown to be sufficiently large that the numerical noise level was acceptable, but we have not revisited this issue within the context of the present simulations for the upgraded machine designs. Whenever M_e exceeds 20,000, the simulation momentarily stops, half of the macroparticles are randomly discarded, and the remaining macroparticles have their charge (and mass) renormalized in such a way that the total physical charge of the ecloud remains unchanged.

Table 1 summarizes the primary input parameters used in our simulations. The left column lists the various cases as specified in "psplusetcparameters" and "lhcupgradeparams" at the time we ran our simulations (late November 2006). Our notation, based on the corresponding input file names, is listed in the 2nd column. The mnemonic is as follows: the number following the name of the machine is the energy in GeV, and the number following "tb" is the bunch spacing in ns, except that "12p5" means 12.5. In addition to the variables defined above, we also list the transverse RMS bunch sizes σ_x and σ_y; their values may be considered averages within the arcs. We assumed a gaussian transverse profile for all cases. The longitudinal profile is listed in the last column.

RESULTS FOR THE LHC

Fig. 2 shows the ecloud heat load vs. $\delta_{\max}$ for all LHC cases considered in this article, except for the short-bunch case ($t_b = 12.5$ ns), whose heat load is much higher than the others (see Fig. 3 for the heat load vs. N_b for this case). It is clear that the long-bunch case leads to the lowest heat load, followed closely by the $t_b = 50$-ns case. It is interesting that this latter case does not show much difference between a flat bunch profile (LHClb2) and a gaussian profile (LCHlb2g).

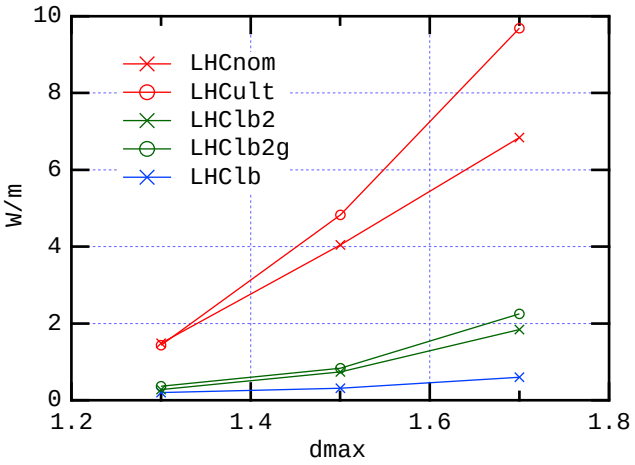

Figure 2: LHC ecloud heat load vs. $\delta_{\max}$ for all cases except LHCsb.

Results for the ecloud heat load as a function of N_b are shown in Fig. 3. The results for the nominal case are more accurate than those shown in Ref. 7 (a detailed report will be published separately). It is clear that the short-bunch case leads to substantial heat load unless $\delta_{\max}$ is rather low. If we take a level of 2 W/m as a rough guide for acceptable heat load, this would require $\delta_{\max} \lesssim 1.1$. The same criterion implies the need for $\delta_{\max} \lesssim 1.3$ for the nominal case. The

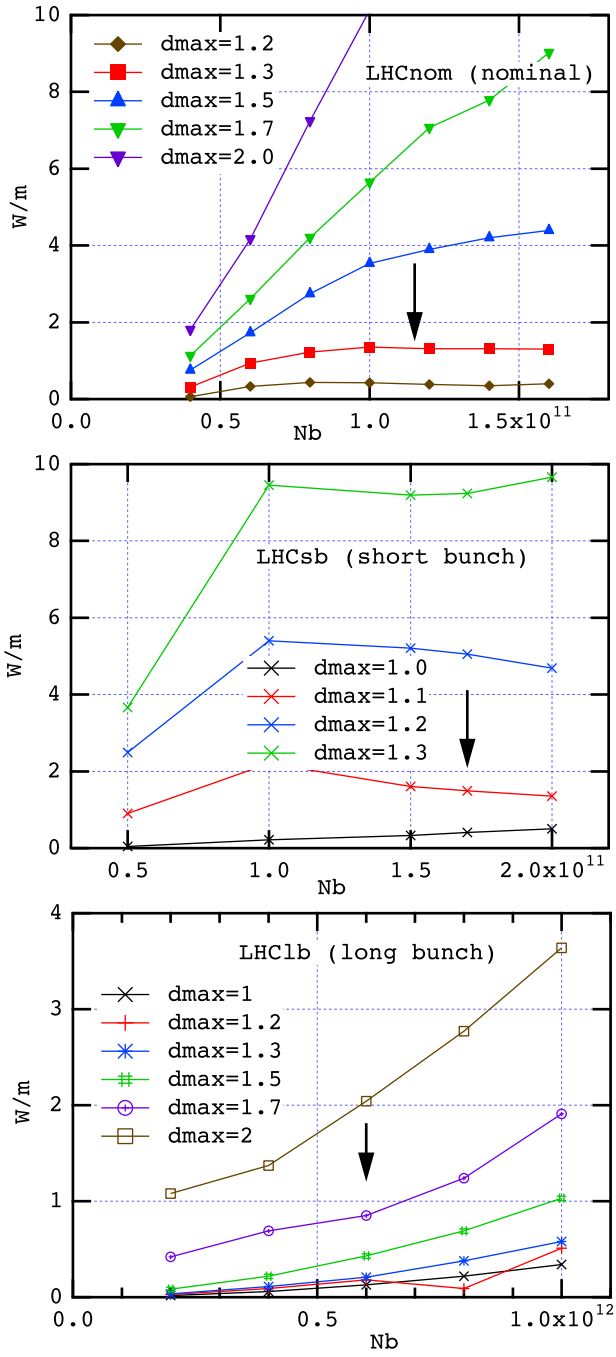

Figure 3: LHC ecloud heat load vs. N_b for various assumed values of the peak SEY $\delta_{\max}$. Top: nominal LHC design. Middle: short bunch option. Bottom: longer bunch option. The black arrow indicates the design value of N_b for each case.

long-bunch case shows, as expected, a very low heat load compared to the others.

RESULTS FOR THE INJECTORS

From the perspective of our present ecloud build-up studies, the only difference between the regular and the

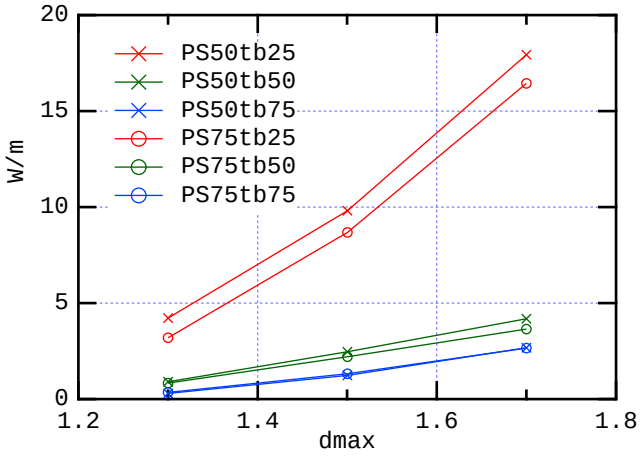

Figure 4: Simulated PS ecloud heat load vs. $\delta_{\max}$ for cases PS50 and PS75 (PS2 and PS+ in "psplusetcparameters," respectively).

"+" cases (see Tab. 1), once the other parameters have been specified, is the transverse size of the vacuum chamber: $(a, b) = (7.0, 2.2)$ cm for the regular cases, and $(a, b) = (6, 2)$ cm for "+" cases. As mentioned above, we have assumed a rectangular stainless steel chamber for all injector options, although we do carry out one comparison between stainless steel and copper.

In all cases we have simulated, the heat load for $t_b = 12.5$ ns is much higher than for the other bunch spacings, hence we have chosen not to display the results for $t_b = 12.5$ ns. Fig. 4 shows a comparison of the ecloud heat load for cases PS50 and PS75, showing relatively small differences between them. Fig. 5 shows a comparison, for the case PS50, between a copper chamber and a stainless steel chamber. In this comparison all simulation parameters, including $\delta_{\max}$, are the same for both cases except for the secondary emission energy spectrum. The remarkably lower simulated heat load for copper can be attributed to the much smaller proportion of rediffused electrons in copper than in stainless steel. The mechanism explaining the difference in heat load is described in Sec. IV of Ref. 7. Fig. 6 shows the simulated heat load for the SPS and SPS+a at 50 GeV, Fig. 7 shows the simulated heat load for the SPS and SPS+b at 75 GeV, and Fig. 8 for the cases $E_b = 450$ and 1,000 GeV.

DISCUSSION

The simulation study presented here for the build-up of the ecloud must be considered a preliminary effort, and is of rather limited scope, as it pertains only to a bending dipole magnet. Furthermore, we have not carried out methodical convergence tests although we believe, from previous studies for the nominal case, that the computational parameters used here (time step, grid size and number of macroparticles) are probably adequate. Except for the $t_b = 25$-ns case in the LHC [7], we have not carried out

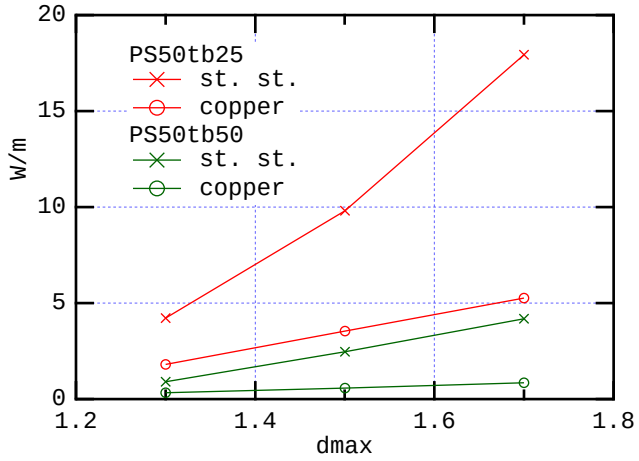

Figure 5: Simulated PS ecloud heat load vs. $\delta_{\max}$ for case PS50, for copper and stainless steel chamber. The only difference in the calculation for the two cases is the secondary emission energy spectrum of the two metals.

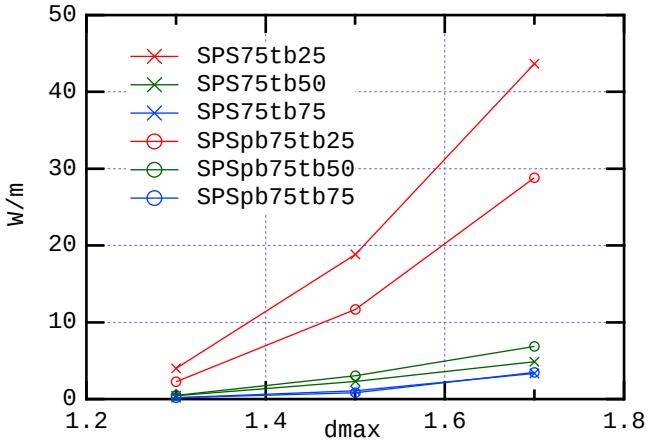

Figure 7: Simulated SPS ecloud heat load vs. $\delta_{\max}$ for cases SPS75 and SPSpb75. The only difference between the calculation for these two cases is the transverse chamber size (see text).

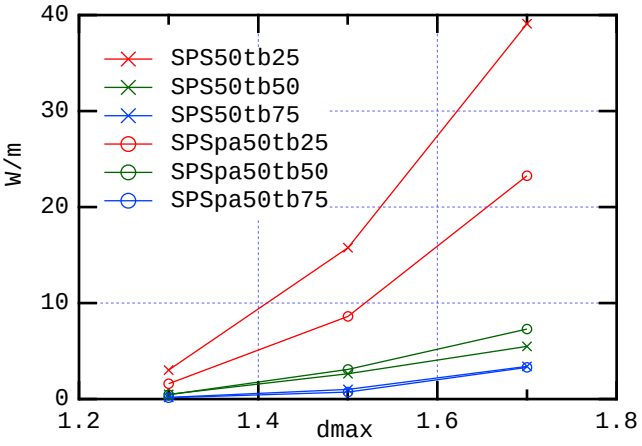

Figure 6: Simulated SPS ecloud heat load vs. $\delta_{\max}$ for cases SPS50 and SPSpa50. The only difference between the calculation for these two cases is the transverse chamber size (see text).

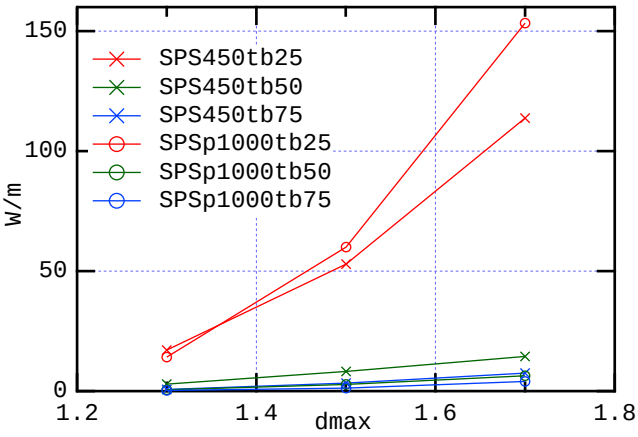

Figure 8: Simulated SPS ecloud heat load vs. $\delta_{\max}$ for $E_b = 450$ GeV and 1 TeV.

parameter sensitivity studies, nor have we looked at convergence of average quantities as a function of physical parameters, notably the bunch train length. Nominal-LHC results show that it takes typically two batches for the ecloud to sensibly reach steady state, and that the average ecloud density computed from the first batch can underestimate the steady-state value by $\sim 40\%$.

For the above reasons, we cannot extract absolute quantitative conclusions from the present simulations; such a goal would require a more detailed, careful analysis, along with experimental calibrations and parameter sensitivity studies. Nevertheless, we can probably conclude with some confidence that the *relative rankings* of the various options are reliable. The rankings extracted from our simulations are:

1. The heat load has a qualitatively inverse relation to bunch spacing t_b: the smaller t_b the higher the heat load, with $t_b = 12.5$ ns leading to a factor 5-10 larger heat load than for $t_b = 25$ ns. Although $t_b = 75$ ns leads to the lowest heat load, the option $t_b = 50$ ns follows closely behind. This ranking is valid both for the LHC and for the injectors.

2. There is not much difference between cases PS50 and PS75 (PS2 and PS+), nor between SPS50 and SPSpa50 (SPS 50 GeV inj. and SPS+a 50 GeV inj.), except at high $\delta_{\max}$ for $t_b = 25$ ns.

3. The simulated heat load for a copper chamber is a clearly lower than for a stainless steel chamber. The origin of this difference is the much lower fraction of rediffused electrons in copper relative to stainless steel in our assumed secondary emission model. It should be emphasized that our results depend directly on the SEY model parameters assumed for these two metals, which were obtained from analysis of bench measure-

ments carried out at different laboratories with different instruments [4, 5]. We do not know if these model parameters actually correspond to the materials used in the vacuum chamber of the machines considered here. Careful emission spectrum measurements carried out under comparable conditions for actual chamber samples would be required to validate the qualitative advantage of copper vis-à-vis stainless steel.

4. Somewhat unexpectedly, there is not much difference in the computed heat load for gaussian vs. flat bunches, at least for the LHC at $t_b = 50$ ns.

In the simulations for the injectors we have assumed a residual gas pressure $P = 10^{-5}$ Torr. Such a high value is intended only as a convenient device to stabilize the simulation of the ecloud build-up against numerical noise and to accelerate it (a more realistic value of P, such as 10^{-9} Torr, would lead to a much higher macroparticle charge or a much larger number of macroparticles in steady state). The assumption made here is that secondary electrons dominate over primary electrons in steady state, hence the primary electron parameters such as P are not very important, within a broad range. We have verified the validity of this assumption for a few cases by computing the heat load with $P = 10^{-5}$ Torr and $\delta_{\max} = 0$. We find that the heat load for the SPS+ at 1 TeV is then ~ 0.7 W/m at $t_b = 25$ ns, and is much lower than this for other cases. While 0.7 W/m is not negligible, it is a factor ~ 10 smaller than what is computed even with $\delta_{\max} = 1.3$ (see Fig. 8).

It appears puzzling that the simulated heat load for the SPS at 450 GeV or 1 TeV at $t_b = 25$ ns (Fig. 8) is a factor of $10 - 20$ times higher than for the LHC nominal case (Fig. 2), also at $t_b = 25$ ns. To try to understand this large difference, we ran simulations for the SPS assuming a SEY model corresponding to copper instead of stainless steel. The results are shown in Fig. 9, which also displays the results for the LHC. We conclude that the heat load for the SPS is now only a factor 2 higher than for the LHC, showing again the remarkable advantage of copper vs. stainless steel (we caution the reader to review item 3 above). We recall that, in the comparison shown in Fig. 9, there are still some differences between the SPS cases and the LHC such as bunch length, chamber geometry and dimensions, primary electron generation mechanism, etc, which account for the remaining factor of 2.

In addition to the heat load, we have also computed other quantities such as electron density (global and close to the beam), ecloud average energy per electron, electron-wall impact energy, and electron flux at the chamber walls. A spreadsheet with all such results is available upon request.

ACKNOWLEDGMENTS

I am grateful to Michael Carrié for his contributions to the LHC upgrade simulations during the summer of 2006; a more complete joint report with such results will be published separately. I am indebted to F. Zimmermann for valuable comments and extensive guidance and clarification of the upgrade parameters for the entire LHC complex, to W. Fischer for many valuable discussions, and to C. Celata for a careful reading of the manuscript. I am grateful to NERSC for supercomputer support.

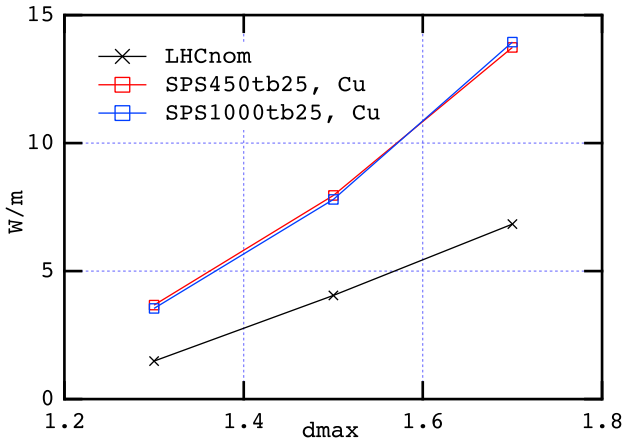

Figure 9: Simulated ecloud heat load for the LHC nominal case and for the SPS+ at $E_b = 450$ and 1,000 GeV vs. $\delta_{\max}$ assuming a SEY model for copper. The bunch spacing is $t_b = 25$ ns in all cases (LHC results taken from Fig. 2).

REFERENCES

[1] CARE-HHH-APD Workshop *Towards a Roadmap for the Upgrade of the CERN and GSI Accelerator Complex* "LHC LUMI 2006," IFIC (Valencia, Spain), 16–20 October 2006, http://care-hhh.web.cern.ch/CARE-HHH/LUMI-06/default.html

[2] M. A. Furman and G. R. Lambertson, "The electron-cloud instability in the arcs of the PEP-II positron ring," LBNL-41123/CBP Note-246, PEP-II AP Note AP 97.27 (Nov. 25, 1997). Proc. *Intl. Workshop on Multibunch Instabilities in Future Electron and Positron Accelerators "MBI-97"* (KEK, 15-18 July 1997; Y. H. Chin, ed.), KEK Proceedings **97-17**, Dec. 1997, p. 170.

[3] M. A. Furman, "The electron-cloud effect in the arcs of the LHC," LBNL-41482/CBP Note 247/LHC Project Report 180 (May 20, 1998).

[4] M. A. Furman and M. T. F. Pivi, "Probabilistic model for the simulation of secondary electron emission," LBNL-49771/CBP Note-415 (Nov. 6, 2002). PRST-AB **5** 124404 (2003), http://prst-ab.aps.org/pdf/PRSTAB/v5/i12/e124404.

[5] M. A. Furman and M. T. F. Pivi, "Simulation of secondary electron emission based on a phenomenological probabilistic model," LBNL-52807/SLAC-PUB-9912 (June 2, 2003).

[6] "LHC Design Report," CERN-2004-003, 4 June 2004.

[7] M. A. Furman and V. H. Chaplin, "Update on electron-cloud power deposition for the Large Hadron Collider arc dipoles," LBNL-59062/CBP Note 723 (January 30, 2006). PRST-AB **9** 034403 (2006), http://prst-ab.aps.org/pdf/PRSTAB/v9/i3/e034403

DISCLAIMER

Table 1: Basic simulation input parameters.

Case	Our notation	E_b GeV	B T	(a,b) cm	N_b 10^{11}	t_b ns	(σ_x,σ_y) mm	σ_z cm	profile ...
PS2, 50 GeV extr.	PS50tb12p5	50	1.8	$(8,4)$	2	12.5	$(1,0.9)$	57.3	gauss.
	PS50tb25	50	1.8	$(8,4)$	4	25	$(1,0.9)$	93.5	gauss.
	PS50tb50	50	1.8	$(8,4)$	5.4	50	$(1,0.9)$	104	flat
	PS50tb75	50	1.8	$(8,4)$	6.6	75	$(1,0.9)$	104	flat
PS+, 75 GeV extr.	PS75tb12p5	75	2.7	$(8,4)$	2	12.5	$(0.8,0.8)$	50.5	gauss.
	PS75tb25	75	2.7	$(8,4)$	4	25	$(0.8,0.8)$	83.5	gauss.
	PS75tb50	75	2.7	$(8,4)$	5.4	50	$(0.8,0.8)$	92.3	flat
	PS75tb75	75	2.7	$(8,4)$	6.6	75	$(0.8,0.8)$	92.3	flat
SPS, 50 GeV inj.	SPS50tb12p5	50	0.225	$(7,2.2)$	1.9	12.5	$(3.1,1.6)$	14.3	gauss.
	SPS50tb25	50	0.225	$(7,2.2)$	3.8	25	$(2.8,1.6)$	23.4	gauss.
	SPS50tb50	50	0.225	$(7,2.2)$	5.2	50	$(3,1.6)$	26.1	flat
	SPS50tb75	50	0.225	$(7,2.2)$	6.4	75	$(3,1.6)$	26.1	flat
SPS, 75 GeV inj.	SPS75tb12p5	75	0.337	$(7,2.2)$	1.9	12.5	$(2.4,1.3)$	12.6	gauss.
	SPS75tb25	75	0.337	$(7,2.2)$	3.8	25	$(2.1,1.3)$	20.9	gauss.
	SPS75tb50	75	0.337	$(7,2.2)$	5.2	50	$(2.3,1.3)$	23.1	flat
	SPS75tb75	75	0.337	$(7,2.2)$	6.4	75	$(2.3,1.3)$	23.1	flat
SPS, 450 GeV extr.	SPS450tb12p5	450	2.025	$(7,2.2)$	1.9	12.5	$(1.2,0.9)$	12	gauss.
	SPS450tb25	450	2.025	$(7,2.2)$	3.8	25	$(1,0.5)$	12	gauss.
	SPS450tb50	450	2.025	$(7,2.2)$	5.2	50	$(1,0.5)$	15	flat
	SPS450tb75	450	2.025	$(7,2.2)$	6.4	75	$(1,0.5)$	15	flat
SPS+, 1 TeV extr.	SPS1000tb12p5	1000	4.5	$(6,2)$	1.8	12.5	$(0.5,0.4)$	12	gauss.
	SPS1000tb25	1000	4.5	$(6,2)$	3.6	25	$(0.6,0.4)$	12	gauss.
	SPS1000tb50	1000	4.5	$(6,2)$	5.1	50	$(0.5,0.4)$	15	flat
	SPS1000tb75	1000	4.5	$(6,2)$	6.2	75	$(0.5,0.4)$	15	flat
SPS+a, 50 GeV inj.	SPSpa50tb12p5	50	0.225	$(6,2)$	1.9	12.5	$(3.1,1.6)$	14.3	gauss.
	SPSpa50tb25	50	0.225	$(6,2)$	3.8	25	$(2.8,1.6)$	23.4	gauss.
	SPSpa50tb50	50	0.225	$(6,2)$	5.2	50	$(3,1.6)$	26.1	flat
	SPSpa50tb75	50	0.225	$(6,2)$	6.4	75	$(3,1.6)$	26.1	flat
SPS+b, 75 GeV inj.	SPSpb75tb12p5	75	0.337	$(6,2)$	1.9	12.5	$(2.4,1.3)$	12.6	gauss.
	SPSpb75tb25	75	0.337	$(6,2)$	3.8	25	$(2.1,1.3)$	20.9	gauss.
	SPSpb75tb50	75	0.337	$(6,2)$	5.2	50	$(2.3,1.3)$	23.1	flat
	SPSpb75tb75	75	0.337	$(6,2)$	6.4	75	$(2.3,1.3)$	23.1	flat
LHC nominal	LHCnom	7000	8.39	$(2.2,1.8)$	1.15	25	$(0.3,0.3)$	7.55	gauss.
LHC ultimate	LHCult	7000	8.39	$(2.2,1.8)$	1.7	25	$(0.3,0.3)$	7.55	gauss.
longer bunch	LHClb	7000	8.39	$(2.2,1.8)$	6	75	$(0.3,0.3)$	14.4	flat
longer bunch 2	LHClb2	7000	8.39	$(2.2,1.8)$	4.9	50	$(0.3,0.3)$	14.4	flat
same except gaussian	LHClb2g	7000	8.39	$(2.2,1.8)$	4.9	50	$(0.3,0.3)$	14.4	gauss.
shorter bunch	LHCsb	7000	8.39	$(2.2,1.8)$	1.7	12.5	$(0.3,0.3)$	3.78	gauss.